

Influence of imperfection on the smart control frequency characteristics of a cylindrical sensor-actuator GPLRC cylindrical shell using a proportional-derivative smart controller

Reza Zare¹, Neda Najaafi², Mostafa Habibi^{*3,4}, Farzad Ebrahimi^{**5} and Hamed Safarpour⁵

¹Department of Electrical Engineering, Shahid Beheshti University, Tehran, Iran

²Iran Industrial Design Company, Tehran, Iran

³Institute of Research and Development, Duy Tan University, Da Nang, 550000, Vietnam

⁴Faculty of Electrical–Electronic Engineering, Duy Tan University, Da Nang, 550000, Vietnam

⁵Mechanical Engineering department, Faculty of Engineering, Imam Khomeini International University, Qazvin, Iran

(Received December 4, 2019, Revised May 31, 2020, Accepted July 12, 2020)

Abstract. This is the first research on the smart control and vibration analysis of a Graphene nanoplatelets (GPLs) Reinforced Composite (GPLRC) porous cylindrical shell covered with piezoelectric layers as sensor and actuator (PLSA) in the framework of numerical based Generalized Differential Quadrature Method (GDQM). The stresses and strains are obtained using the First-order Shear Deformable Theory (FSDT). Rule of the mixture is employed to obtain varying mass density and Poisson's ratio, while the module of elasticity is computed by modified Halpin-Tsai model. The external voltage is applied to sensor layer and a Proportional-Derivative (PD) controller is used for sensor output control. Governing equations and boundary conditions of the GPLRC cylindrical shell are obtained by implementing Hamilton's principle. The results show that PD controller, length to radius ratio (L/R), applied voltage, porosity and weight fraction of GPL have significant influence on the frequency characteristics of a porous GPLRC cylindrical shell. Another important consequence is that at the lower value of the applied voltage, the influence of the smart controller on the frequency of the micro composite shell is much more significant in comparison with the higher ones.

Keywords: sensor and actuator; PD controller; imperfection; cylindrical shell; frequency characteristics

1. Introduction

Due to the never-ending attitude of technology (Chen *et al.* 2020, Shen *et al.* 2016, Wang and Chen 2020, Wang *et al.* 2017, Xu and Chen 2014, Xu *et al.* 2019, Zhao *et al.* 2014, 2019) for improving the mechanical properties and operation of the structures, GPL reinforcement gains the attention of scientists for providing an enthusiastic enhancement in the design of the applicable composite structures (Habibi *et al.* 2019a, c, Hashemi *et al.* 2019, Safarpour *et al.* 2020). Sun and Zhao (2018) compared the fracture behavior of the Functionally Graded (FG) cemented carbide reinforced with and without the GPLs. They claimed that the property of GPLs in the nanocomposites is worked as a stopper for micro cracks. In addition, with the aid of an experimental study, Rafiee *et al.* (2009) reported that the polymer matrix composite which is reinforced by GPL is much stronger than the reinforced structures with Single-Walled Carbon Nanotube (SWCNT), Double-Walled Carbon Nanotube (DWCNT) and Multi-

Walled Carbon Nanotube (MWCNT). In recent years it was notable that the nano pants fortified by GPLs are much more useful in engineering applications, based on this matter the dynamic behavior of the nanostructures reinforced with GPL is a momentous field of study. In the mentioned field of study, Yang *et al.* (2017) investigated the stability and instability responses of the FG nanobeams reinforced with GPLs. They showed that the GPLs can make a positive contribution to the buckling and post-buckling behavior of the nanostructure. In the other paper, Feng *et al.* (2017) focused on the nonlinear bending behavior of the composite smart beams reinforced with GPLs. They claimed that the beam with a higher volume fraction of the GPLs with symmetric distribution in such way is less sensitive to the nonlinear deformation.

The high strength and stiffness of GPLs and CNTs make them as the applicable reinforcements in comparison with conventional fibers used in compositionally shell, beam, and plate. In the mentioned field of study, Yas *et al.* (2013) conducted a study on free vibration of CNTs reinforced FG nanocomposite panel employing Generalized Differential Quadrature (GDQ) method into governing equations established based on the 3D elasticity theory. Shen *et al.* (2017, 2018a, b) conducted a study on nonlinear dynamic response and bending behavior of the FG-GPLRC laminated cylindrical shell and exposed to thermal environment using shear deformation theory. They

*Corresponding author, Ph.D.,
E-mail: mostafahabibi@duytan.edu.vn

**Co-corresponding author, Professor,
E-mail: febrahimi@eng.ikiu.ac.ir

considered nonlinearity effect with the aid of von Kármán model and solved the mathematical problem based on the two-step perturbation. Wang *et al.* (2018) presented the free vibrational behavior of the FG-GPLRC doubly curved shallow shells by employing Navier technique on the basic equations extracted from Hamilton principle. Kumari and Kar (2019) used Pagano's technique and modified Kantorovich approach to obtain an analytical solution to static problem of composite shell panel with applied arbitrary boundary conditions at each edge. Free vibration and buckling behavior of initially stressed FG-GPLRC cylindrical shell using state-space technique within the framework of three-dimensional elasticity was probed by Liu *et al.* (2018).

It is worth mentioning, in all of these studies, the porosities' effect in composite materials was ignored. Due to porosities occurring inside composites during manufacture process, it is necessary to consider porosities' phenomena in vibration analysis of structures. The porous materials are composed of two elements: One element is solid (body) and the other is either gas or liquid that is frequently found in nature, such as dust layers, stone, and wood. In the past years, material of porous structures, such as shells, plates, and beam, has been widely discussed in design of structural problems. Some researchers (Alimirzaei *et al.* 2019, Hashemi *et al.* 2019) investigated the vibration of porous composite structures.

Piezoelectric materials produce electric potential and elastic deformations as response to mechanical pressure and imposed electric field. The most usage of piezoelectric layers is found in smart structures for distributed sensors and actuators to control deformations and noise as well as suppress vibrations. On the other hand, applications of piezoelectric materials in operational environments with converse conditions resulted in advent of new branch of advanced inhomogeneous composite materials known as Functionally Graded Materials (FGMs). In FGMs, properties continuously vary through the specific directions according to a designated function. This distinctive characteristic allows such composite materials to have higher thermal and corrosion resistance and hinder stress concentrations caused by interface-mismatch between properties of dissimilar materials (Koizumi 1993). Accordingly, combination of FGMs and piezoelectric materials provided a fantastic opportunity to present an innovative class of smart materials. For these reasons, the investigation of mechanical response of FG and also FG laminated piezoelectric structures has drawn considerable attention to research which some of the related references are briefly described as follows. Many researches showed the advantage of various deformation theory (Addou *et al.* 2019, Boukhelif *et al.* 2019, Boulefrakh *et al.* 2019, Boutaleb *et al.* 2019, Khiloun *et al.* 2019, Mahmoudi *et al.* 2019, Zaoui *et al.* 2019, Zarga *et al.* 2019). Ebrahimi and Rastgoo (2008a) studied the vibrational responses of the FG circular plate which is actuated with the aid of the piezoelectric layer. They modeled two direct FG plate based on the classical plate theory. In the other work, they focused on the dynamic responses of the annular FG plate actuated with piezo materials (Ebrahimi and Rastgoo 2008b), employing

the high order deformation theory is necessary for modeling the thick structures (Abualnour *et al.* 2019, Belbachir *et al.* 2019, Bourada *et al.* 2019, Chaabane *et al.* 2019, Hellal *et al.* 2019, Meksi *et al.* 2019, Tlidji *et al.* 2019). Duc and Van Tung (2010) considered the von Karman effect for serving the nonlinear geometric in the mathematical modeling of the FG panels. Stability and instability of the size dependent structure are presented in Refs (Alimirzaei *et al.* 2019, Bedia *et al.* 2019, Berghouti *et al.* 2019; Boutaleb *et al.* 2019, Draoui *et al.* 2019, Hussain *et al.* 2019, Karami *et al.* 2019a, b, c, Medani *et al.* 2019; Semmah *et al.* 2019, Tlidji *et al.* 2019). Alibeigloo (2013) focused on the bending characteristics of a CNT reinforced FG plate which is covered with piezoelectric actuator and sensor. In addition, they considered a mechanical load along the length of the structures and solve the problem with the aid of 3D elasticity theory.

In the field of vibration control of the smart structures, Hajmohammad *et al.* (2018) focused on the control and vibrational behavior of the laminated conical nanoshell. The nanostructure is covered with piezoelectric sensor and actuator then the dynamic response of the nanocomposite is improved by using a PD controller. In addition, they modeled a PD controller for serving a smart controller on the deflection of the structure. They presented that consideration the PD controller can contribute to decrease the maximum displacement and time of the instability of the structure. Chuaqui *et al.* (2018) presented the vibrational behavior of an Al-beam covered with piezoelectric sensor and actuator. Mehrvarz *et al.* (2018) investigated the smart vibration control of a microbeam with the aid of strain gradient theory, and they derived governing equations and boundary conditions using Hamilton's principle. Vatankhah *et al.* (2015) focused on the investigation of the vibro smart control of the cantilever micro beam by employing the piezoelectric sensor and actuator and robust linear controller. They solved the PDE equations of the problem using the Galerkin method. They showed that the stability of the nano smart structures improves by using robust linear controller. In the field of dynamics response of the porous structures, some researchers showed that this parameter decrease the frequency of the structures (Addou *et al.* 2019, Alimirzaei *et al.* 2019, Berghouti *et al.* 2019, Medani *et al.* 2019). In addition, in the recent year we can see that some research (Chen *et al.* 2020, Ghabussi *et al.* 2019, Moayedi *et al.* 2018, 2019, Moayedi and Hayati 2018a, b, Moayedi and Rezaei 2019, Shen *et al.* 2016, Wang and Chen 2020, Wang *et al.* 2017, Xu and Chen 2014, Xu *et al.* 2019, Zhao *et al.* 2014, 2019) are presented on the soft computing methods for prediction the behavior of different structures.

To the best of authors' knowledge, smart control and frequency analysis of a porous GPLRC cylindrical shell covered with piezoelectric layers as sensor and actuator has not been issued in the published literature. In this study, modified Halpin-Tsai micromechanics is employed to approximate effective elastic properties. Numerical solution to differential governing equations is presented in the case of various boundary conditions. Special attentions are given to explore the effects of PD controller, length to radius ratio (L/R), applied voltage and weight fraction of GPL on the

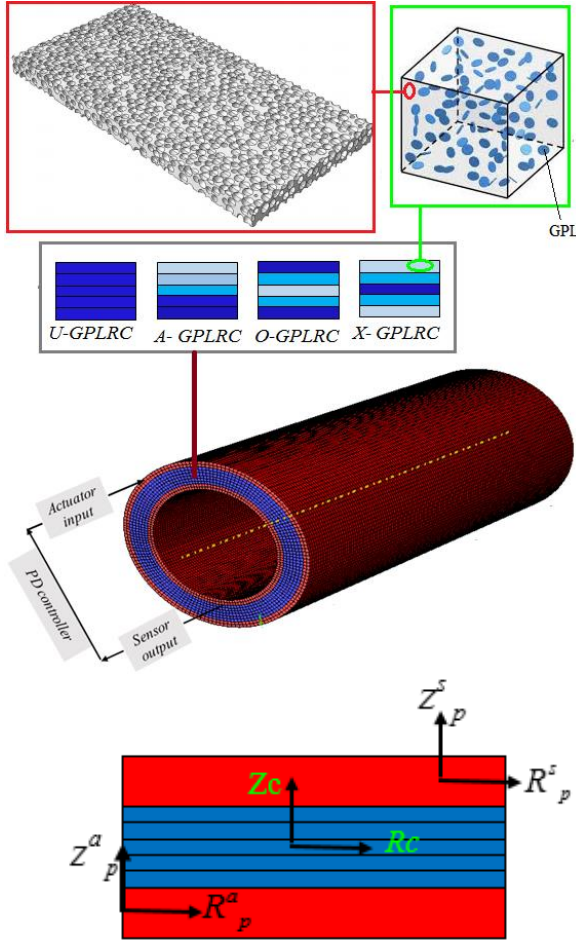


Fig. 1 Schematic of a porous GPLRC cylindrical shell integrated with sensor and actuator layers

frequency characteristics of a smart porous GPLRC cylindrical shell covered with PLSA.

2. Theory and formulation

A GPLRC cylindrical shell integrated with sensor and actuator layers is shown in Fig. 1. In addition, a PD controller is used for vibration control of the structure. As depicted in the Fig. 1, four patterns are considered for modeling the GPLRC materials for reinforcement of the structures. The volume fraction functions for each diagram are expressed as (Song *et al.* 2017)

$$U - GPLRC: V_{GPL}(k) = V_{GPL}^* \quad (1)$$

$$X - GPLRC: V_{GPL}(k) = 2V_{GPL}^* |2k - N_L - 1| / N_L \quad (2)$$

$$O - GPLRC: V_{GPL}(k) = 2V_{GPL}^* [1 - (|2k - N_L - 1| / N_L)] \quad (3)$$

$$A - GPLRC: V_{GPL}(k) = 2V_{GPL}^* (2k - 1) / N_L \quad (4)$$

The parameters that are used in Eqs. (1)-(4) are given in Song *et al.* (2017) in detail. The relation between V_{GPL}^* and its weight fraction g_{GPL} can be obtained by

$$V_{GPL}^* = \frac{g_{GPL}}{g_{GPL} + (\rho_{GPL} / \rho_m)(1 - g_{GPL})} \quad (5)$$

in which ρ_{GPL} and ρ_m are the mass densities of the GPL and polymer matrix. The effective modulus of elasticity of GPLRC shell is estimated using modified Halpin-Tsai micromechanics (De Villoria and Miravete 2007).

$$E = \left(\frac{3}{8} \left(\frac{1 + \xi_L \eta_L V_{GPL}}{1 - \eta_L V_{GPL}} \right) + \frac{5}{8} \left(\frac{1 + \xi_W \eta_W V_{GPL}}{1 - \eta_W V_{GPL}} \right) \right) \times E_M \quad (6)$$

$$\xi_L = 2 \frac{L_{GPL}}{t_{GPL}}, \quad \xi_W = 2 \frac{W_{GPL}}{t_{GPL}}$$

$$\eta_L = \frac{\left(\frac{E_{GPL}}{E_M} \right) - 1}{\left(\frac{E_{GPL}}{E_M} \right) + \xi_L}, \quad \eta_W = \frac{\left(\frac{E_{GPL}}{E_M} \right) - 1}{\left(\frac{E_{GPL}}{E_M} \right) + \xi_W}$$

Finally, by using the rule of mixture, mass density ρ_c and Poisson's ratio ν_c of the GPL/polymer micro composite are expressed as

$$\begin{aligned} \nu &= \nu_{GPL} V_{GPL} + \nu_M V_M \\ \rho &= \rho_{GPL} V_{GPL} + \rho_M V_M \end{aligned} \quad (7)$$

The mechanical properties of the porous FG-GPLRC cylindrical shell with different types of porosity distributions can be obtained by Sahmani *et al.* (2018)

$$\begin{aligned} E_{eff} &= \bar{E} [1 - \Gamma_p S(z)] \\ \rho_{eff} &= \bar{\rho} [1 - \Gamma_m S(z)] \\ v_{eff} &= 0.221 \left(1 - \frac{\rho_{eff}}{\bar{\rho}} \right) + \bar{\nu} \left[\frac{1 + 0.342 \left(1 - \frac{\rho_{eff}}{\bar{\rho}} \right)^2}{-1.21 \left(1 - \frac{\rho_{eff}}{\bar{\rho}} \right)} \right] \end{aligned} \quad (8)$$

where

$$S(z) = \begin{cases} \cos\left(\frac{\pi z}{2h} + \frac{\pi}{4}\right) & \text{for porosity distribution 1} \\ \cos\left(\frac{\pi z}{h}\right) & \text{for porosity distribution 2} \\ 1 - \cos\left(\frac{\pi z}{h}\right) & \text{for porosity distribution 3} \end{cases} \quad (9)$$

It is noted that, Eq. (8) is modelled for the porous structure with two-dimensional stress-strain relationship. Based on the Gaussian random field scheme (Roberts and Garboczi 2001), the coefficient of mass density (Γ_m) can be defined as a function of Γ_m as follows

$$\Gamma_m = 1.121 [1 - (1 - \Gamma_p S(z))^{1/2.3}] / S(z) \quad (10)$$

2.1 Mathematical modeling of the structure

With the aid of the First-order Shear Deformation Theory (FSDT) (Alimirzaei *et al.* 2019, Draiche *et al.* 2019, Draoui *et al.* 2019, Medani *et al.* 2019, Semmah *et al.*

2019), the displacement fields of the core (cylindrical shell) are expressed by the following equations

$$\begin{aligned} u(x, \theta, z, t) &= u_0(x, \theta, t) + z\psi_x(x, \theta, t) \\ v(x, \theta, z, t) &= v_0(x, \theta, t) + z\psi_\theta(x, \theta, t) \\ w(x, \theta, z, t) &= w_0(x, \theta, t) \end{aligned} \quad (11)$$

where displacement fields in Eq. (11) are discussed in detail in Esmailpoor Hajilak *et al.* (2019). Constitutive equations for nanocomposite core and piezoelectric layers.

The 3D stress-strain relation of the GPLRC core can be obtained as below

$$\begin{bmatrix} \sigma_{xx} \\ \sigma_{\theta\theta} \\ \sigma_{x\theta} \\ \sigma_{xz} \\ \sigma_{\theta z} \end{bmatrix} = \begin{bmatrix} \bar{Q}_{11} & \bar{Q}_{12} & 0 & 0 & 0 \\ \bar{Q}_{21} & \bar{Q}_{22} & 0 & 0 & 0 \\ 0 & 0 & \bar{Q}_{66} & 0 & 0 \\ 0 & 0 & 0 & \bar{Q}_{55} & 0 \\ 0 & 0 & 0 & 0 & \bar{Q}_{44} \end{bmatrix} \begin{bmatrix} \varepsilon_{xx} \\ \varepsilon_{\theta\theta} \\ \varepsilon_{x\theta} \\ \varepsilon_{xz} \\ \varepsilon_{\theta z} \end{bmatrix} \quad (12)$$

2.2 Piezoelectric layers

According to the FSDT, displacement fields of the piezoelectric layers are assumed as follows

$$\begin{aligned} u_p^i(x, \theta, z, t) &= u_{0p}^i(x, \theta, z) + zu_{1p}^i(x, \theta, z) \\ v_p^i(x, \theta, z, t) &= v_{0p}^i(x, \theta, z) + zv_{1p}^i(x, \theta, z) \\ w_p^i(x, \theta, z, t) &= w_{0p}^i(x, \theta, z, t) \end{aligned} \quad (13)$$

The relationships between the stress and strain for the piezoelectric layers (sensor and actuator) are written as below

$$\begin{bmatrix} \sigma_{xx} \\ \sigma_{\theta\theta} \\ \sigma_{x\theta} \\ \sigma_{\theta z} \\ \sigma_{xz} \end{bmatrix} = \begin{bmatrix} c_{11} & c_{12} & 0 & 0 & 0 \\ c_{12} & c_{22} & 0 & 0 & 0 \\ 0 & 0 & c_{66} & 0 & 0 \\ 0 & 0 & 0 & c_{55} & 0 \\ 0 & 0 & 0 & 0 & c_{44} \end{bmatrix} \begin{bmatrix} \varepsilon_{xx} \\ \varepsilon_{\theta\theta} \\ \varepsilon_{x\theta} \\ \varepsilon_{\theta z} \\ \varepsilon_{xz} \end{bmatrix} - \begin{bmatrix} 0 & 0 & e_{31}^i \\ 0 & 0 & e_{32}^i \\ 0 & 0 & 0 \\ 0 & e_{24}^i & 0 \\ e_{25}^i & 0 & 0 \end{bmatrix} \begin{bmatrix} E_x^i \\ E_\theta^i \\ E_z^i \end{bmatrix} - \begin{bmatrix} \beta_{11}^i \\ \beta_{22}^i \\ 0 \\ 0 \\ 0 \end{bmatrix} \Delta T \quad (14)$$

$$\begin{bmatrix} D_x^i \\ D_\theta^i \\ D_z^i \end{bmatrix} = \begin{bmatrix} 0 & 0 & 0 & 0 & e_{15}^i \\ 0 & 0 & 0 & e_{24}^i & 0 \\ e_{31}^i & e_{32}^i & 0 & 0 & 0 \end{bmatrix} \begin{bmatrix} \varepsilon_{xx} \\ \varepsilon_{\theta\theta} \\ \varepsilon_{x\theta} \\ \varepsilon_{\theta z} \\ \varepsilon_{xz} \end{bmatrix} + \begin{bmatrix} s_{11}^i & 0 & 0 \\ 0 & s_{22}^i & 0 \\ 0 & 0 & s_{33}^i \end{bmatrix} \begin{bmatrix} E_x^i \\ E_\theta^i \\ E_z^i \end{bmatrix} + \begin{bmatrix} p_1^i \\ p_2^i \\ p_3^i \end{bmatrix} \Delta T, \quad (15)$$

$i = a, s$

So

$$\begin{aligned} D_x^i &= e_{15}\varepsilon_{xz} + s_{11}E_x \\ &= e_{15} \left(\psi_x + \frac{\partial w_0^i}{\partial x} \right) - s_{11} \left(\sin(\beta) \frac{\partial \phi^i}{\partial x} \right) \end{aligned} \quad (16)$$

$$\begin{aligned} D_\theta^i &= e_{24}\varepsilon_{\theta z} + s_{22}E_\theta = e_{24} \left(\psi_\theta + \frac{1}{R} \frac{\partial w_0^i}{\partial \theta} - \frac{v_0^i}{R} \right) \\ &\quad - s_{22} \left(\frac{1}{R+z} \sin\left(\frac{\pi(z-t^c/2)}{t^t}\right) \frac{\partial \phi^i}{\partial \theta} \right) \\ D_z^i &= e_{31}\varepsilon_{xx} + e_{32}\varepsilon_{\theta\theta} + s_{33}E_z = e_{31} \left(\frac{\partial u_0^i}{\partial x} + z \frac{\partial u_1^i}{\partial x} \right) \\ &\quad + e_{32} \left(\frac{1}{R} \frac{\partial v_0^i}{\partial \theta} + \frac{z}{R} \frac{\partial v_1^i}{\partial \theta} + \frac{w_0^i}{R} \right) \\ &\quad - s_{33} \left(\cos\left(\frac{\pi(z-t^c/2)}{t^t}\right) \left(\frac{\pi}{t^t} \phi^i \right) + \frac{V_0}{t^t} \right) \end{aligned}$$

In Eqs. (15) and (16), c_{ijkl} , e_{mij} , d_{in} , p_i , β_{ij} and s_{im} are the elasticity matrix, piezo-electric, pyro-electric constants, thermal module, and dielectric constants, respectively. Other parameters are discussed in Safarpour *et al.* (2019a, b) in detail. The electric and magnetic field strength which are used in Eqs. (15) and (16), can be expressed as below

$$\begin{aligned} E_x^i &= -\frac{\partial \Phi^i}{\partial x}, & E_\theta^i &= -\frac{1}{R+z} \frac{\partial \Phi^i}{\partial \theta} \\ E_z^i &= -\frac{\partial \Phi^i}{\partial z} \end{aligned} \quad (17)$$

Hajmohammad *et al.* (2018) investigated that the potential of electric along sensor and actuator directions can be assumed as

$$\begin{aligned} \phi^a(x, \theta, z, t) &= \sin\left(\frac{\pi(z-t^c/2)}{t^t}\right) \phi^a(x, \theta, t) + \frac{(z-t^c/2)V_0}{t^t} \\ \phi^s(x, \theta, z, t) &= \sin\left(\frac{\pi(-z-t^c/2)}{t^b}\right) \phi^s(x, \theta, t) \end{aligned} \quad (18)$$

It is noted that the current smart structure is only polarized along the direction of thickness. ϕ^a and ϕ^s are the initial external electric along with actuator and sensor layers, respectively. Moreover, $\phi^i(x, \theta, t)$ is a spatial variation of the electric potential in x and θ directions, respectively. Also, V_0 is the initial external electric potential. Now by substituting Eq. (18) into Eq. (17), we have

$$\begin{aligned} E_x^a &= -\sin\left(\frac{\pi(z-t^c/2)}{t^t}\right) \frac{\partial \phi^a}{\partial x} \\ E_\theta^a &= -\frac{1}{R+z} \sin\left(\frac{\pi(z-t^c/2)}{t^t}\right) \frac{\partial \phi^a}{\partial \theta} \\ E_z^a &= -\cos\left(\frac{\pi(z-t^c/2)}{t^t}\right) \left(\frac{\pi}{t^t} \phi^a \right) - \frac{V_0}{t^t} \\ E_x^s &= -\sin\left(\frac{\pi(-z-t^c/2)}{t^b}\right) \frac{\partial \phi^s}{\partial x} \\ E_\theta^s &= -\frac{1}{R+z} \sin\left(\frac{\pi(-z-t^c/2)}{t^b}\right) \frac{\partial \phi^s}{\partial \theta} \\ E_z^s &= -\cos\left(\frac{\pi(-z-t^c/2)}{t^b}\right) \left(-\frac{\pi}{t^b} \phi^s \right) \end{aligned} \quad (19)$$

2.3 Compatibility equations

It assumes perfect bonding between the core and the piezoelectric layer, $z_p = -h_p/2$ are as follow (Eyvazian *et al.* 2019, Motezaker and Eyvazian 2020a, b)

$$\begin{aligned}
 u_c(z_c = h_c/2) &= u_p^a(z_p^a = -h_p^a/2) \\
 v_c(z_c = h_c/2) &= v_p^a(z_p^a = -h_p^a/2) \\
 w_c(z_c = h_c/2) &= w_p^a(z_p^a = -h_p^a/2) \\
 u_c(z_c = -h_c/2) &= u_p^s(z_p^s = h_p^s/2) \\
 v_c(z_c = -h_c/2) &= v_p^s(z_p^s = h_p^s/2) \\
 w_c(z_c = -h_c/2) &= w_p^s(z_p^s = h_p^s/2)
 \end{aligned} \tag{20}$$

To obtain the equations of motion and boundary conditions, Hamilton’s principle is utilized, so, it can be written as (Habibi *et al.* 2019, Moayedi *et al.* 2020)

$$\int_{t_1}^{t_2} (\delta T_1 + \delta T_2 - \delta U_1 - \delta U_2 + \delta W_1 + \delta W_2) dt = 0 \tag{21}$$

Strain energy: The strain energy of GPLRC cylindrical shell with piezoelectric layers can be divided as follows.

Strain energy of the piezoelectric layers is

$$\begin{aligned}
 U_1 &= \frac{1}{2} \iiint_{V_{piezolayer}} (\sigma_{ij} \varepsilon_{ij}) dV_{piezolayer} \\
 &- \iiint_{V_{piezolayer}} (D_x \delta E_x + D_\theta \delta E_\theta + D_z \delta E_z) dV_{piezolayer} \\
 &- D_x^a \left(\sin\left(\frac{\pi(z - \frac{t^c}{2})}{t^t}\right) \frac{\partial \delta \phi^a}{\partial x} \right) - D_\theta^a \left(\frac{1}{R+z} \right. \\
 &\left. \sin\left(\frac{\pi(z - \frac{t^c}{2})}{t^t}\right) \frac{\partial \delta \phi^a}{\partial \theta} \right) + D_z^a \left(\cos\left(\frac{\pi(z - \frac{t^c}{2})}{t^t}\right) \right. \\
 &\left. \left(\frac{\pi}{t^t} \delta \phi^a \right) \right) - D_x^s \left(\sin\left(\frac{\pi(-z - \frac{t^c}{2})}{t^b}\right) \frac{\partial \delta \phi^s}{\partial x} \right) \\
 &- D_\theta^s \left(\frac{1}{R+z} \sin\left(\frac{\pi(-z - \frac{t^c}{2})}{t^b}\right) \frac{\partial \delta \phi^s}{\partial \theta} \right) \\
 &+ D_z^s \left(\cos\left(\frac{\pi(-z - \frac{t^c}{2})}{t^b}\right) \left(\frac{\pi}{t^b} \delta \phi^s \right) \right)
 \end{aligned} \tag{22a}$$

In Eq. (22) ε_{ij} and σ_{ij} represent the components of the strain and stress tensors and presented as follow.

Strain energy of the core is

$$U_1 = \frac{1}{2} \iiint_{V_{Core}} (\sigma_{ij} \varepsilon_{ij}) dV_{Core} \tag{22b}$$

Kinetic energy: The kinetic energy for each layer can be defined as below

$$\delta K = (1 - \mu^2 \nabla^2) \int_Z \int_A \rho \left\{ \begin{aligned} &\left(\frac{\partial u^\lambda}{\partial t} + z \frac{\partial \psi^\lambda_x}{\partial t} \right) \times \\ &\left(\frac{\partial}{\partial t} \delta u^\lambda + z \frac{\partial}{\partial t} \delta \psi^\lambda_x \right) \\ &+ \left(\frac{\partial v^\lambda}{\partial t} + z \frac{\partial \psi^\lambda_\theta}{\partial t} \right) \times \\ &\left(\frac{\partial}{\partial t} \delta v^\lambda + z \frac{\partial}{\partial t} \delta \psi^\lambda_\theta \right) \\ &+ \left(\frac{\partial w^\lambda}{\partial t} \right) \frac{\partial}{\partial t} \delta w^\lambda \end{aligned} \right\} dV \tag{23}$$

Work done: The first variation of the work done corresponding to the external electric applied force of the sensor layer

$$\delta W_1 = \iint_A \left[(N_1^{Ps}) w_{,x} \delta w_{,x} \right. \\ \left. + (N_2^{Ps}) v_{,x} \delta v_{,x} \right] R_{sensorlayer} dx d\theta \tag{24}$$

where N_{ip} is external electric loads. The electric loads could be obtained as follows.

$$N_1^P = N_2^P = -2(e_{31} - \frac{c_{13}e_{33}}{c_{33}}) \phi_0 \tag{25}$$

Governing equations for a GPLRC cylindrical shell covered with Piezoelectric sensor actuator based on the FSDT by substituting Eqs. (22), (23) and (24) into Eq. (21) than integrating by parts can be obtained. It should be noted that, based on Eq. (20) the numbers of unknown variables are decreased from 15 to 9. So, the total number of unknowns in the face sheets and core are reduced to 9.

3. Solution procedure

At this stage, a numerical technique (Chen *et al.* 2020, Wang *et al.* 2017, Xu *et al.* 2019) with the aids of GDQM method is introduced to investigate the vibrational characteristics of a circular microplate. In this computational technique, the n th order derivatives of an adequately smooth function f with respect to corresponding discrete points within the overall domain can be estimated as a weighted linear sum of the function values at all the discrete mesh points in the whole domain as follows (Shu 2012)

$$\frac{\partial^n f}{\partial r^n} = \sum_{m=1}^M C^{(n)}_{j,m} f_{m,k} \tag{26}$$

where $C^{(n)}$ are weighting coefficients for the n th-order derivative along the radius direction. As it can be noticed from Eq. (26), the key part of DQM lies in computing the weighting coefficients. For this purpose, two types of DQM composed of GDQM are adopted in this study to approximate the n th order derivatives of function along radius direction. In addition, $C^{(n)}$ are calculated as below from the first-order derivative

$$\begin{aligned}
 C_{ij}^{(1)} &= \frac{M(x_i)}{(x_i - x_j)M(x_j)} \quad i, j = 1, 2, \dots, n \text{ and } i \neq j \\
 C_{ij}^{(1)} &= - \sum_{j=1, j \neq i}^n C_{ij}^{(1)} \quad i = j
 \end{aligned} \tag{27}$$

where

$$M(x_i) = \prod_{j=1, j \neq i}^n (x_i - x_j) \tag{28}$$

In addition, the weighting coefficients for higher-order

derivatives are developed by the following relations.

$$\begin{aligned}
 C_{ij}^{(r)} &= r \left[C_{ij}^{(r-1)} C_{ij}^{(1)} - \frac{C_{ij}^{(r-1)}}{(x_i - x_j)} \right] \\
 i, j &= 1, 2, \dots, n, i \neq j \text{ and } 2 \leq r \leq n-1 \\
 C_{ii}^{(r)} &= - \sum_{j=1, i \neq j}^n C_{ij}^{(r)} \\
 i, j &= 1, 2, \dots, n \text{ and } 1 \leq r \leq n-1
 \end{aligned} \tag{29}$$

In the present study, a non-uniform set of seeds is chosen along x and θ directions as follows.

$$r_i = \frac{L}{2} \left(1 - \cos \left(\frac{(i-1)}{(N_i-1)} \pi \right) \right) \quad i = 1, 2, 3, \dots, N_i \tag{30}$$

Rearranging the quadrature analogs of field equations and boundary conditions inside the fabric of a generalized eigenvalue problem yield

$$\left\{ \begin{aligned} & \left[\begin{array}{cc} [M_{dd}] & [M_{db}] \\ [M_{bd}] & [M_{bb}] \end{array} \right] \omega^2 \\ & + \left[\begin{array}{cc} [K_{dd}] & [K_{db}] \\ [K_{bd}] & [K_{bb}] \end{array} \right] \end{aligned} \right\} \begin{Bmatrix} \delta_d \\ \delta_b \end{Bmatrix} = 0 \tag{31}$$

in which the subscripts b and d refer to the boundary and domain grid points, respectively. By applying a PD controller, the following relation for the sensor output can be written as follows

$$\phi^a = G_d \phi^s + G_v \dot{\phi}^s \tag{32}$$

where G_d and G_v are proportional and derivative control coefficients, respectively. Finally, with setting Eq. (31) to

zero, we can obtain natural frequency of the structure. In addition, dimensionless critical voltage is defined as follows (Wang and Reddy 2014)

$$\begin{aligned}
 \bar{\phi} &= \frac{10 \times \phi}{\sqrt{\frac{A_{11}}{X_{33}}}} \\
 X_{33} &= \int_{-h/2}^{h/2} \{s_{33e}\} (\beta \sin(\beta z))^2 dz
 \end{aligned} \tag{33}$$

4. Results section

4.1 Convergency

The sufficient number of grid points is necessary to achieve accurate results in GDQM. The convergence studies are conducted for different boundary conditions as well as different materials. Moreover, it can be seen that the structure with Clamped-Clamped (C-C) boundary conditions is stiffer than the structure with Simply-Simply (S-S) boundary conditions which will lead to a smaller natural frequency. Also, GPLRC cylindrical shell, due to the addition of GPL reinforcing nanofillers has a higher natural frequency in comparison to pure epoxy. According to Table 1, for results convergence, eleven grid points are suitable.

4.2 Validation

To assess validity and accuracy of the approaches in this study for frequency analysis, numerical results are compared with those of Ref. (Wang et al. 2014) in Table 2 for a piezoelectric cylindrical shell and for different mode reported from the table which implies that the maximum

Table 1 The effect of the number of grid points on the results convergence for the natural frequency (GHz) of the GPLRC shell with respect to different patterns and Boundary Conditions (B. Cs) when $L/R = 10$, $h/R = 0.1$, $l = R/3$ and $h/h_p = 10$

B. Cs	Material	N = 5	N = 7	N = 9	N = 11	N = 13	Analytical results
S-S	Pure epoxy	0.586990	0.600494	0.600154	0.600157	0.600157	0.60015788945
	Pattern 1	0.753884	0.771359	0.770919	0.770923	0.770923	0.77092377091
	Pattern 2	0.753446	0.770921	0.770482	0.770483	0.770486	0.77048629174
	Pattern 3	0.754608	0.772089	0.771649	0.771649	0.771653	0.77165393069
	Pattern 4	0.753915	0.771394	0.770954	0.770958	0.770958	0.77095861186
C-S	Pure epoxy	1.015471	0.988214	0.989878	0.990481	0.990481	-
	Pattern 1	1.315586	1.277954	1.280044	1.280673	1.280673	-
	Pattern 2	1.315153	1.277527	1.279621	1.280250	1.280250	-
	Pattern 3	1.316584	1.278919	1.281002	1.281631	1.281631	-
	Pattern 4	1.315836	1.278088	1.280175	1.280815	1.280815	-
C-C	Pure epoxy	1.690101	1.520517	1.521102	1.521473	1.521473	-
	Pattern 1	2.203252	1.978261	1.979007	1.979982	1.979982	-
	Pattern 2	2.202765	1.977791	1.978537	1.979009	1.979009	-
	Pattern 3	1.204738	1.979634	1.980378	1.980847	1.980847	-
	Pattern 4	2.203561	1.978344	1.979085	1.979550	1.979550	-

Table 2 Comparison of the natural frequencies (GHz) of piezoelectric cylindrical nanoshells for various circumferential wave numbers (n) with $m = 1$, $L/R = 12$, $R/h = 50$, and $l = 0$

n	Ke <i>et al.</i> (2014a, b)	Present	Error (%)
1	0.7188	0.70794	1.51
2	0.4101	0.4080	0.51
3	0.8003	0.78697	1.67
4	1.4793	1.46632	0.87
5	2.3723	2.35491	0.73
6	3.4695	3.44352	0.74
7	4.7685	4.72918	0.82
8	6.2687	6.20995	0.93
9	7.9694	7.88407	0.11
10	9.8707	9.74973	0.12

discrepancy between the results is approximately 1%. As well as this, it can be seen that by increasing the mode number, the natural frequency tends to decrease and then increase. As another validation, Table 3 compares the results for dimensionless natural frequency of a cylindrical shell with different distribution patterns, between the reported results with those obtained by Liu *et al.* (2018), for different geometrical parameters. The static and dynamic gains of the PD controller are obtained by Matlab software as $G_d = 0.455$ and $G_v = 0.6$, respectively.

4.3 Material properties

In the current study, the GPLRC structure with a thickness of $h_{GPL} = 1.5$ nm, length of $a_{GPL} = 2.5$ nm and Radius of $R_{GPL} = 0.75$ nm is modeled. The mechanical properties of the GPL and epoxy are given in Table 4. In addition, the material properties of the piezoelectric layers are given in Safarpour *et al.* (2019a, b).

4.4 Results and discussion

Fig. 2 illustrates the effects of the smart controller and applied voltage through the thickness of the piezoelectric sensor and actuator on the vibrational behavior of the structure for S-S and C-C boundary conditions. As an astonishing and applicable result for having a suitable prediction about the behavior, control, and operation of the composite structure which can be seen from Fig. 2 is that, at the lower value of the applied voltage, the influence of the smart controller on the frequency of the nanocomposite

Table 4 Material properties of the epoxy and GPL (Wu *et al.* 2017)

Material properties	Epoxy	GPL
Young's modulus (GPa)	3	1010
Density (kg m ⁻³)	1200	1062.5
Poisson's ratio	0.34	0.186

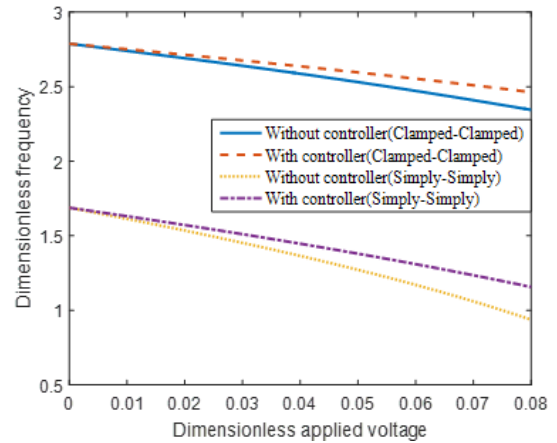


Fig. 2 The effects of the smart controller and applied voltage on the natural frequency for different boundary conditions

shell is much more significant in comparison with the higher ones. By having more attention to this figure, at the higher value of the applied voltage, the positive effect of the employing smart piezoelectric sensor and actuator controller has appeared for both C-C and S-S boundary conditions. It is obvious that not only can see an improvement from a smart piezoelectric sensor and actuator controller on the stability of the structure but also this phenomenon is much more remarkable for S-S in comparison with C-C boundary condition. Figs. 3, 4 and 5 show the influence of nonlocal parameter (μ/R), PD smart controller, and g_{GPL} on the natural frequency of the GPLRC smart shell with C-C, C-S and S-S boundary conditions.

The more common result which these figures confirm is that, for all boundary conditions and different values of the g_{GPL} , by increasing the μ/R parameter, the natural frequency of the GPLRC smart shell decreases exponentially. According to these figures, the remarkable result is that by increasing the value of the g_{GPL} encounters us with an improvement in the dynamic responses of the smart structure. In addition, when the controller is

Table 3 Comparison of the dimensionless natural frequency of GPLRC nanoshells, considering different parameters

$m\pi L/l_{GPL}$	Epoxy	Epoxy present (Liu <i>et al.</i> 2018)	GPL-UD (Liu <i>et al.</i> 2018)	GPL-UD present	GPL-A (Liu <i>et al.</i> 2018)	GPL-A present
2	0.9659	0.9365985	2.3674	2.303659	2.2517	2.242659
5	2.6997	2.6698544	6.6185	6.486598	5.4878	5.463265
10	5.6503	5.6265987	13.8540	13.80756	9.6421	9.635698

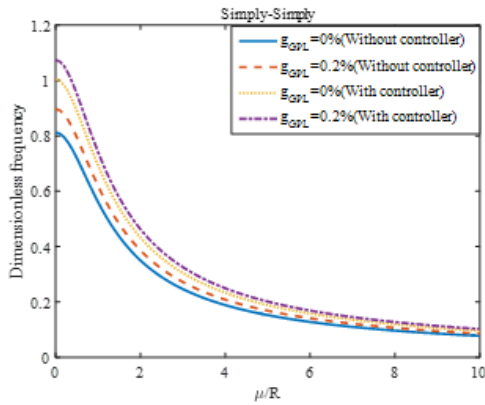


Fig. 3 The effects of the smart controller, nonlocal parameter, and g_{GPL} on the natural frequency of the GPLRC smart shell for S-S boundary conditions

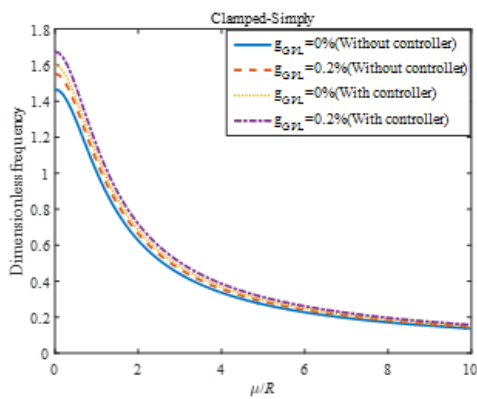


Fig. 4 The effects of the smart controller, nonlocal parameter and g_{GPL} on the natural frequency of the GPLRC smart shell for the C-S boundary conditions

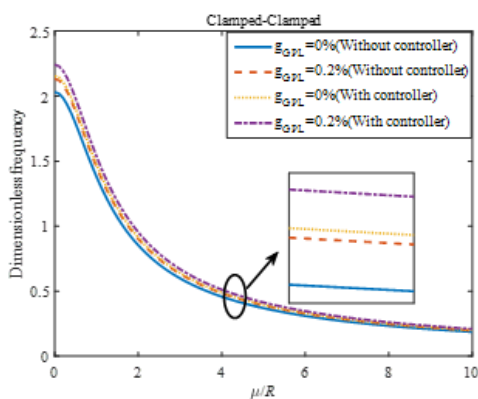


Fig. 5 The effects of the smart controller, nonlocal parameter and g_{GPL} on the natural frequency of the GPLRC smart shell for the C-C boundary conditions

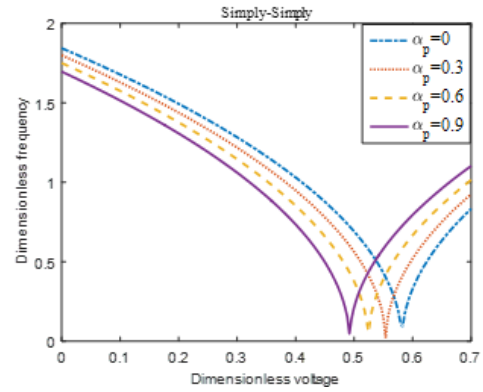


Fig. 6 The effects of the applied voltage and different porosity coefficients on the natural frequency of the GPLRC smart shell for the S-S boundary conditions

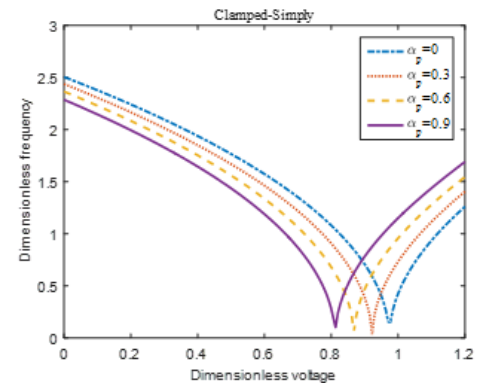


Fig. 7 The effects of the applied voltage and different porosity coefficients on the natural frequency of the GPLRC smart shell for the C-S boundary conditions

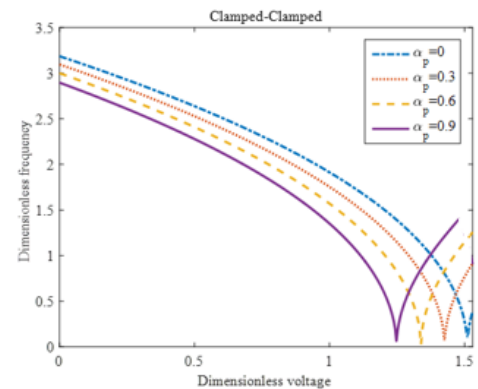


Fig. 8 The effects of the applied voltage and different porosity coefficients on the natural frequency of the GPLRC smart shell for the C-C boundary conditions

considered, the improvement of the stability of the smart shell from increasing the g_{GPL} is less than the condition which there is not considered the controller. In other words,

by considering the controller the positive effect of g_{GPL} on the frequency is not remarkable in comparison without controller. The best result from these fingers is that, when the boundary condition changes from S-S to C-C, the

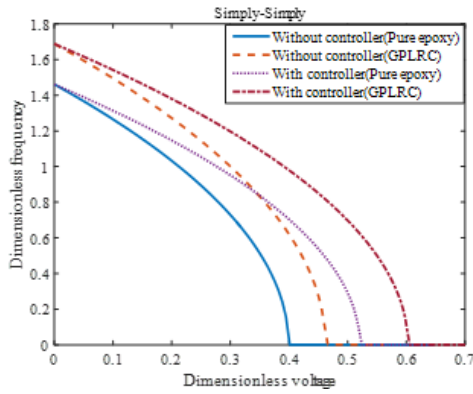


Fig. 9 The effects of the smart controller, applied voltage, and GPL reinforcement on the natural frequency of the GPLRC smart shell for the S-S boundary condition

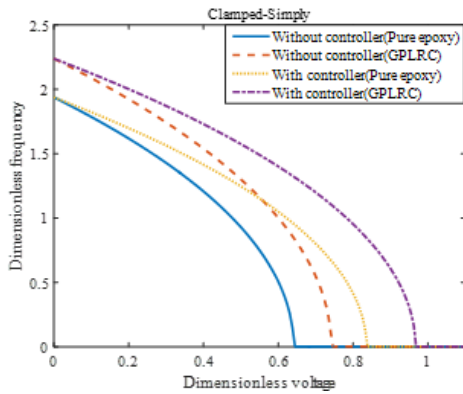


Fig. 10 The effects of the smart controller, applied voltage, and GPL reinforcement on the natural frequency of the GPLRC smart shell for the C-S boundary condition

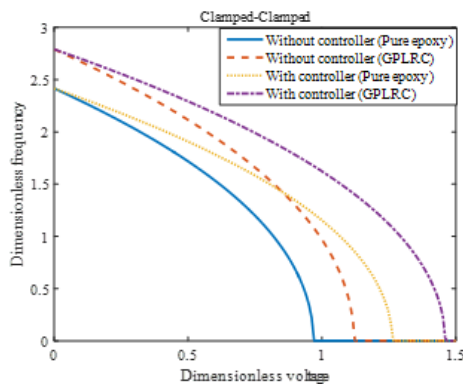


Fig. 11 The effects of the smart controller, applied voltage, and GPL reinforcement on the natural frequency of the GPLRC smart shell for the C-C boundary condition

affirmative effect of the smart controller and g_{GPL} on the frequency decreases. For more comprehensive, by increasing the rigidity at boundary domains (changing boundary conditions from S-S to C-C), the effect of

controller and GPL reinforcement on the frequency decrease. Figs. 6, 7 and 8 encounter us with a presentation about the effects of the applied voltage and different porosity coefficients (α_p) on the natural frequency of the smart GPL reinforced shell for C-C, C-S and S-S boundary conditions.

According to the above figures, the main result is that increasing the porosity coefficient leads to a decrease the critical applied voltage of the GPLRC smart shell for all boundary conditions and these phenomena are intensified when the boundary conditions of the structure change from S-S to C-C. Figs. 9, 10 and 11 encounter us with a presentation about the effects of the smart controller, applied voltage, and GPL reinforcement on the natural frequency of the smart shell for C-C, C-S and S-S boundary conditions

Possessed in common result is that when the core of the structure changes from pure epoxy to GPLRC, the dynamic stability or natural frequency of the structure and critical dimensionless voltage increase simultaneously, due to adding a little bit of GPL into pure epoxy as a reinforcement. The main result which comes up from Figs. 9, 10 and 11 is that considering the smart controller causes to increase in the critical applied voltage and frequency of the system for both pure epoxy and GPLRC shell. As an astonishing result for the literature, for a specific value of the dimensionless voltage, the natural frequency of the pure epoxy shell integrated with piezoelectric sensor and actuator and GPLRC shell without controller is equaled so that this matter proves that by employing the smart controller can design a simple structure (pure epoxy shell) for the desired application instead of the complex composite (GPLRC) shell.

5. Conclusions

This study focused on presenting a numerical solution for control vibration analysis of a GPLRC porous cylindrical shell covered with sensor and actuator layers. Governing differential motion equations were solved using Hamilton's principle. Validation of the obtained results was examined by comparing them with those published in the available literature. The results show that the PD controller, applied voltage and g_{GPL} have a significant influence on the frequency characteristics of the porous GPLRC cylindrical shell. The numerical results revealed that:

- At the lower value of the applied voltage, the influence of the smart controller on the frequency of the micro composite shell is much more significant in comparison with the higher ones.
- The results demonstrate that the natural frequency of the structure goes up when the PD controller is considered.
- The best result from these fingers is that, when the boundary condition changes from S-S to C-C, the affirmative effect of the smart controller and g_{GPL} on the frequency decreases.
- Increase in the porosity coefficient leads to a decrease in the critical applied voltage of the GPLRC smart shell for all boundary conditions and these phenomena are

intensified when the boundary conditions of the structure change from S-S to C-C.

Acknowledgments

We would like to acknowledge the reviewers for their helpful comments on this research.

References

- Alimirzaei, S., Mohammadimehr, M. and Tounsi, A. (2019), "Nonlinear analysis of viscoelastic micro-composite beam with geometrical imperfection using FEM: MSGT electro-magneto-elastic bending, buckling and vibration solutions", *Struct. Eng. Mech., Int. J.*, **71**(5), 485-502. <https://doi.org/10.12989/sem.2019.71.5.485>.
- Bedia, W.A., Houari, M.S.A., Bessaim, A., Bousahla, A.A., Tounsi, A., Saeed, T. and Alhodaly, M.S. (2019), "A new hyperbolic two-unknown beam model for bending and buckling analysis of a nonlocal strain gradient nanobeams", *J. Nano Res.*, **57**, 175-191. <https://doi.org/10.4028/www.scientific.net/JNanoR.57.175>.
- Belbachir, N., Draich, K., Bousahla, A.A., Bourada, M., Tounsi, A. and Mohammadimehr, M. (2019), "Bending analysis of anti-symmetric cross-ply laminated plates under nonlinear thermal and mechanical loadings", *Steel Compos. Struct., Int. J.*, **33**(1), 81-92. <https://doi.org/10.12989/scs.2019.33.1.081>.
- Berghouti, H., Adda Bedia, E., Benkhedda, A. and Tounsi, A. (2019), "Vibration analysis of nonlocal porous nanobeams made of functionally graded material", *Adv. Nano Res., Int. J.*, **7**(5), 351-364. <https://doi.org/10.12989/anr.2019.7.5.351>.
- Boukhelif, Z., Bouremana, M., Bourada, F., Bousahla, A.A., Bourada, M., Tounsi, A. and Al-Osta, M.A. (2019), "A simple quasi-3D HSDT for the dynamics analysis of FG thick plate on elastic foundation", *Steel Compos. Struct., Int. J.*, **31**(5), 503-516. <https://doi.org/10.12989/scs.2019.31.5.503>.
- Boulefrakh, L., Hebali, H., Chikh, A., Bousahla, A.A., Tounsi, A. and Mahmoud, S. (2019), "The effect of parameters of visco-Pasternak foundation on the bending and vibration properties of a thick FG plate", *Geomech. Eng., Int. J.*, **18**(2), 161-178. <https://doi.org/10.12989/gae.2019.18.2.161>.
- Bourada, F., Bousahla, A.A., Bourada, M., Azzaz, A., Zinata, A. and Tounsi, A. (2019), "Dynamic investigation of porous functionally graded beam using a sinusoidal shear deformation theory", *Wind Struct., Int. J.*, **28**(1), 19-30. <https://doi.org/10.12989/was.2019.28.1.019>.
- Boutaleb, S., Benrahou, K.H., Bakora, A., Algarni, A., Bousahla, A.A., Tounsi, A., Tounsi, A. and Mahmoud, S. (2019), "Dynamic analysis of nanosize FG rectangular plates based on simple nonlocal quasi 3D HSDT", *Adv. Nano Res., Int. J.*, **7**(3), 191. <https://doi.org/10.12989/anr.2019.7.3.191>.
- Chaabane, L.A., Bourada, F., Sekkal, M., Zerouati, S., Zaoui, F. Z., Tounsi, A., Derras, A., Bousahla, A. and Tounsi, A. (2019), "Analytical study of bending and free vibration responses of functionally graded beams resting on elastic foundation", *Struct. Eng. Mech., Int. J.*, **71**(2), 185-196. <https://doi.org/10.12989/sem.2019.71.2.185>.
- Chen, H., Zhang, Q., Luo, J., Xu, Y. and Zhang, X. (2020), "An enhanced bacterial foraging optimization and its application for training kernel extreme learning machine", *Appl. Soft Comput.*, **86**, 105884. <https://doi.org/10.1016/j.asoc.2019.105884>.
- Chuaqui, T.R., Roque, C.M. and Ribeiro, P. (2018), "Active vibration control of piezoelectric smart beams with radial basis function generated finite difference collocation method", *J. Intell. Mater. Syst. Struct.*, **29**(13), 2728-2743. <https://doi.org/10.1016/j.asoc.2019.105884>.
- De Villoria, R.G. and Miravete, A. (2007), "Mechanical model to evaluate the effect of the dispersion in nanocomposites", *Acta Materialia*, **55**(9), 3025-3031. <https://doi.org/10.1016/j.actamat.2007.01.007>.
- Draiche, K., Bousahla, A.A., Tounsi, A., Alwabli, A.S., Tounsi, A. and Mahmoud, S. (2019), "Static analysis of laminated reinforced composite plates using a simple first-order shear deformation theory", *Comput. Concr., Int. J.*, **24**(4), 369-378. <https://doi.org/10.12989/cac.2019.24.4.369>.
- Draoui, A., Zidour, M., Tounsi, A. and Adim, B. (2019), "Static and dynamic behavior of nanotubes-reinforced sandwich plates using (FSDT)", *J. Nano Res.*, **57**, 117-135. <https://doi.org/10.4028/www.scientific.net/JNanoR.57.117>.
- Duc, N.D. and Van Tung, H. (2010), "Nonlinear analysis of stability for functionally graded cylindrical panels under axial compression", *Comput. Mater. Sci.*, **49**(4), 313-316. <https://doi.org/10.1016/j.commatsci.2009.12.030>.
- Ebrahimi, F. and Rastgoo, A. (2008a), "An analytical study on the free vibration of smart circular thin FGM plate based on classical plate theory", *Thin-Wall. Struct.*, **46**(12), 1402-1408. <https://doi.org/10.1016/j.tws.2008.03.008>.
- Ebrahimi, F. and Rastgoo, A. (2008b), "Free vibration analysis of smart annular FGM plates integrated with piezoelectric layers", *Smart Mater. Struct.*, **17**(1), 015044. <https://doi.org/10.1088/0964-1726/17/1/015044>.
- Esmailpoor Hajilak, Z., Pourghader, J., Hashemabadi, D., Sharifi Bagh, F., Habibi, M. and Safarpour, H. (2019), "Multilayer GPLRC composite cylindrical nanoshell using modified strain gradient theory", *Mech. Des. Struct. Mach.*, 1-25. <https://doi.org/10.1080/15397734.2019.1566743>.
- Eyvazian, A., Hamouda, A.M., Tarlochan, F., Mohsenizadeh, S. and Dastjerdi, A.A. (2019), "Damping and vibration response of viscoelastic smart sandwich plate reinforced with non-uniform Graphene platelet with magnetorheological fluid core", *Steel Compos. Struct., Int. J.*, **33**(6), 891-906. <https://doi.org/10.12989/scs.2019.33.6.891>.
- Feng, C., Kitipornchai, S. and Yang, J. (2017), "Nonlinear bending of polymer nanocomposite beams reinforced with non-uniformly distributed graphene platelets (GPLs)", *Compos. Part B Eng.*, **110**, 132-140. <https://doi.org/10.1016/j.compositesb.2016.11.024>.
- Ghabussi, A., Ashrafi, N., Shavalipour, A., Hosseinpour, A., Habibi, M., Moayedi, H., Babaei, B. and Safarpour, H. (2019), "Free vibration analysis of an electro-elastic GPLRC cylindrical shell surrounded by viscoelastic foundation using modified length-couple stress parameter", *Mech. Based Des. Struct. Mach.*, 1-25. <https://doi.org/10.1080/15397734.2019.1705166>.
- Habibi, M., Hashemabadi, D. and Safarpour, H. (2019a), "Vibration analysis of a high-speed rotating GPLRC nanostructure coupled with a piezoelectric actuator", *Eur. Phys. J. Plus*, **134**(6), 307. <https://doi.org/10.1140/epjp/i2019-12742-7>.
- Habibi, M., Mohammadi, A., Safarpour, H. and Ghadiri, M. (2019b), "Effect of porosity on buckling and vibrational characteristics of the imperfect GPLRC composite nanoshell", *Mech. Based Des. Struct. Mach.*, 1-30. <https://doi.org/10.1080/15397734.2019.1701490>.
- Habibi, M., Mohammadi, A., Safarpour, H., Shavalipour, A. and Ghadiri, M. (2019c), "Wave propagation analysis of the laminated cylindrical nanoshell coupled with a piezoelectric actuator", *Mech. Based Des. Struct. Mach.*, 1-19. <https://doi.org/10.1080/15397734.2019.1697932>.
- Hajmohammad, M.H., Farrokhi, A. and Kolahchi, R. (2018), "Smart control and vibration of viscoelastic actuator-multiphase nanocomposite conical shells-sensor considering hygrothermal

- load based on layerwise theory”, *Aerosp. Sci. Technol.*, **78**, 260-270. <https://doi.org/10.1016/j.ast.2018.04.030>.
- Hashemi, H.R., Alizadeh, A.A., Oyarhossein, M.A., Shavalipour, A., Makkiabadi, M. and Habibi, M. (2019), “Influence of imperfection on amplitude and resonance frequency of a reinforcement compositionally graded nanostructure”, *Waves Random Complex Media*, 1-27. <https://doi.org/10.1080/17455030.2019.1662968>.
- Hellal, H., Bourada, M., Hebali, H., Bourada, F., Tounsi, A., Bousahla, A.A. and Mahmoud, S. (2019), “Dynamic and stability analysis of functionally graded material sandwich plates in hygro-thermal environment using a simple higher shear deformation theory” *J. Sandw. Struct. Mater.*, 1099636219845841. <https://doi.org/10.1177/1099636219845841>.
- Hussain, M., Naeem, M.N., Tounsi, A. and Taj, M. (2019), “Nonlocal effect on the vibration of armchair and zigzag SWCNTs with bending rigidity”, *Adv. Nano Res., Int. J.*, **7**(6), 431-442. <https://doi.org/10.12989/anr.2019.7.6.431>.
- Karami, B., Janghorban, M. and Tounsi, A. (2019a), “Galerkin’s approach for buckling analysis of functionally graded anisotropic nanoplates/different boundary conditions”, *Eng. Comput.*, **35**(4), 1297-1316. <https://doi.org/10.1007/s00366-018-0664-9>.
- Karami, B., Janghorban, M. and Tounsi, A. (2019b), “On pre-stressed functionally graded anisotropic nanoshell in magnetic field”, *J. Braz. Soc. Mech. Sci. Eng.*, **41**(11), 495. <https://doi.org/10.1007/s40430-019-1996-0>.
- Karami, B., Janghorban, M. and Tounsi, A. (2019c), “Wave propagation of functionally graded anisotropic nanoplates resting on Winkler-Pasternak foundation”, *Struct. Eng. Mech., Int. J.*, **70**(1), 55-66. <https://doi.org/10.12989/sem.2019.70.1.055>.
- Karami, B., Shahsavari, D., Janghorban, M. and Tounsi, A. (2019d), “Resonance behavior of functionally graded polymer composite nanoplates reinforced with graphene nanoplatelets”, *Int. J. Mech. Sci.*, **156**, 94-105. <https://doi.org/10.1016/j.ijmecsci.2019.03.036>.
- Ke, L.L., Wang, Y.S., Yang, J. and Kitipornchai, S. (2014a), “The size-dependent vibration of embedded magneto-electro-elastic cylindrical nanoshells”, *Smart Mater. Struct.*, **23**(12), 125036. <https://doi.org/10.1088/09641726/23/12/125036/meta>.
- Ke, L., Wang, Y. and Reddy, J. (2014b), “Thermo-electro-mechanical vibration of size-dependent piezoelectric cylindrical nanoshells under various boundary conditions”, *Compos. Struct.*, **116**, 626-636. <https://doi.org/10.1016/j.compstruct.2014.05.048>.
- Khiloun, M., Bousahla, A.A., Kaci, A., Bessaim, A., Tounsi, A. and Mahmoud, S. (2019), “Analytical modeling of bending and vibration of thick advanced composite plates using a four-variable quasi 3D HSDT”, *Eng. Comput.*, 1-15. <https://doi.org/10.1007/s00366-019-00732-1>.
- Kumari, P. and Kar, S. (2019), “Static behavior of arbitrarily supported composite laminated cylindrical shell panels: An analytical 3D elasticity approach”, *Compos. Struct.*, **207**, 949-965. <https://doi.org/10.1016/j.compstruct.2018.09.035>.
- Liu, D., Kitipornchai, S., Chen, W. and Yang, J. (2018), “Three-dimensional buckling and free vibration analyses of initially stressed functionally graded graphene reinforced composite cylindrical shell”, *Compos. Struct.*, **189**, 560-569. <https://doi.org/10.1016/j.compstruct.2018.01.106>.
- Mahmoudi, A., Benyoucef, S., Tounsi, A., Benachour, A., Adda Bedia, E.A. and Mahmoud, S. (2019), “A refined quasi-3D shear deformation theory for thermo-mechanical behavior of functionally graded sandwich plates on elastic foundations”, *J. Sandw. Struct. Mater.*, **21**(6), 1906-1929. <https://doi.org/10.1177/1099636217727577>.
- Medani, M., Benahmed, A., Zidour, M., Heireche, H., Tounsi, A., Bousahla, A.A., Tounsi, A. and Mahmoud, S. (2019), “Static and dynamic behavior of (FG-CNT) reinforced porous sandwich plate using energy principle”, *Steel Compos. Struct., Int. J.*, **32**(5), 595-610. <https://doi.org/10.12989/scs.2019.32.5.595>.
- Mehrvarz, A., Salarieh, H., Alasty, A. and Vatankhah, R. (2018), “Boundary vibration control of strain gradient Timoshenko micro-cantilevers using piezoelectric actuators”, *arXiv*, 1812.01155.
- Meksi, R., Benyoucef, S., Mahmoudi, A., Tounsi, A., Adda Bedia, E.A. and Mahmoud, S. (2019), “An analytical solution for bending, buckling and vibration responses of FGM sandwich plates”, *J. Sandw. Struct. Mater.*, **21**(2), 727-757. <https://doi.org/10.1177/1099636217698443>.
- Moayedi, H. and Hayati, S. (2018a), “Applicability of a CPT-based neural network solution in predicting load-settlement responses of bored pile”, *Int. J. Geomech.*, **18**(6), 06018009. [https://doi.org/10.1061/\(ASCE\)GM.1943-5622.0001125](https://doi.org/10.1061/(ASCE)GM.1943-5622.0001125).
- Moayedi, H. and Hayati, S. (2018b), “Modelling and optimization of ultimate bearing capacity of strip footing near a slope by soft computing methods”, *Appl. Soft Comput.*, **66**, 208-219. <https://doi.org/10.1016/j.asoc.2018.02.027>.
- Moayedi, H. and Rezaei, A. (2019), “An artificial neural network approach for under-reamed piles subjected to uplift forces in dry sand”, *Neural Comput. Appl.*, **31**(2), 327-336. <https://doi.org/10.1007/s00521-017-2990-z>.
- Moayedi, H., Bui, D.T., Gör, M., Pradhan, B. and Jaafari, A. (2019), “The feasibility of three prediction techniques of the artificial neural network, adaptive neuro-fuzzy inference system, and hybrid particle swarm optimization for assessing the safety factor of cohesive slopes”, *ISPRS Int. J. Geo-Inf.*, **8**(9), 391. <https://doi.org/10.3390/ijgi8090391>.
- Moayedi, H., Darabi, R., Ghabussi, A., Habibi, M. and Foong, L.K. (2020), “Weld orientation effects on the formability of tailor welded thin steel sheets”, *Thin-Wall. Struct.*, **149**, 106669. <https://doi.org/10.1016/j.tws.2020.106669>.
- Motezaker, M. and Eyvazian, A. (2020a), “Buckling load optimization of beam reinforced by nanoparticles”, *Struct. Eng. Mech., Int. J.*, **73**(5), 481-486. <https://doi.org/10.12989/sem.2020.73.5.481>.
- Motezaker, M. and Eyvazian, A. (2020b), “Post-buckling analysis of Mindlin Cut out-plate reinforced by FG-CNTs”, *Steel Compos. Struct., Int. J.*, **34**(2), 289-297. <https://doi.org/10.12989/scs.2020.34.2.289>.
- Rafiee, M.A., Rafiee, J., Wang, Z., Song, H., Yu, Z.Z. and Koratkar, N. (2009), “Enhanced mechanical properties of nanocomposites at low graphene content”, *ACS Nano*, **3**(12), 3884-3890. <https://doi.org/10.1021/nn9010472>.
- Roberts, A.P. and Garboczi, E.J. (2001), “Elastic moduli of model random three-dimensional closed-cell cellular solids”, *Acta Materialia*, **49**(2), 189-197. [https://doi.org/10.1016/S1359-6454\(00\)00314-1](https://doi.org/10.1016/S1359-6454(00)00314-1).
- Safarpour, H., Ghanbari, B. and Ghadiri, M. (2019a), “Buckling and free vibration analysis of high speed rotating carbon nanotube reinforced cylindrical piezoelectric shell”, *Appl. Math. Model.*, **65**, 428-442. <https://doi.org/10.1016/j.apm.2018.08.028>.
- Safarpour, H., Pourghader, J. and Habibi, M. (2019b), “Influence of spring-mass systems on frequency behavior and critical voltage of a high-speed rotating cantilever cylindrical three-dimensional shell coupled with piezoelectric actuator”, *J. Vib. Control*, **25**(9), 1543-1557. <https://doi.org/10.1177/1077546319828465>.
- Safarpour, M., Ghabussi, A., Ebrahimi, F., Habibi, M. and Safarpour, H. (2020), “Frequency characteristics of FG-GPLRC viscoelastic thick annular plate with the aid of GDQM”, *Thin-Wall. Struct.*, **150**, 106683.

- <https://doi.org/10.1016/j.tws.2020.106683>.
- Sahmani, S., Aghdam, M.M. and Rabczuk, T. (2018), "Nonlocal strain gradient plate model for nonlinear large-amplitude vibrations of functionally graded porous micro/nano-plates reinforced with GPLs", *Compos. Struct.*, **198**, 51-62. <https://doi.org/10.1016/j.compstruct.2018.05.031>.
- Semmah, A., Heireche, H., Bousahla, A.A. and Tounsi, A. (2019), "Thermal buckling analysis of SWBNNT on Winkler foundation by non local FSDT", *Adv. Nano Res., Int. J.*, **7**(2), 89-98. <https://doi.org/10.12989/anr.2019.7.2.089>.
- Shen, H.S., Xiang, Y. and Fan, Y. (2017), "Nonlinear vibration of functionally graded graphene-reinforced composite laminated cylindrical shells in thermal environments", *Compos. Struct.*, **182**, 447-456. <https://doi.org/10.1016/j.compositesb.2017.10.032>.
- Shen, L., Chen, H., Yu, Z., Kang, W., Zhang, B., Li, H., Yang, B. and Liu, D. (2016), "Evolving support vector machines using fruit fly optimization for medical data classification", *Knowl. Based Syst.*, **96**, 61-75. <https://doi.org/10.1016/j.knosys.2016.01.002>.
- Shen, H.S., Xiang, Y., Fan, Y. and Hui, D. (2018a), "Nonlinear bending analysis of FG-GRC laminated cylindrical panels on elastic foundations in thermal environments", *Compos. Part B Eng.*, **141**, 148-157. <https://doi.org/10.1016/j.compositesb.2017.12.048>.
- Shen, H.S., Xiang, Y., Fan, Y. and Hui, D. (2018b), "Nonlinear vibration of functionally graded graphene-reinforced composite laminated cylindrical panels resting on elastic foundations in thermal environments", *Compos. Part B Eng.*, **136**, 177-186. <https://doi.org/10.1016/j.compositesb.2017.10.032>.
- Shu, C. (2012), *Differential Quadrature and its Application in Engineering*, Springer Science & Business Media, London, UK.
- Song, M., Kitipornchai, S. and Yang, J. (2017), "Free and forced vibrations of functionally graded polymer composite plates reinforced with graphene nanoplatelets", *Compos. Struct.*, **159**, 579-588. <https://doi.org/10.1016/j.compstruct.2016.09.070>.
- Sun, J. and Zhao, J. (2018), "Multi-layer graphene reinforced nano-laminated WC-Co composites", *Mater. Sci. Eng. A*, **723**, 1-7. <https://doi.org/10.1016/j.msea.2018.03.040>.
- Tlidji, Y., Zidour, M., Draiche, K., Safa, A., Bourada, M., Tounsi, A. and Mahmoud, S. (2019), "Vibration analysis of different material distributions of functionally graded microbeam", *Struct. Eng. Mech., Int. J.*, **69**(6), 637-649. <https://doi.org/10.12989/sem.2019.69.6.637>.
- Vatankhah, R., Nojournian, M.A. and Salarieh, H. (2015), "Vibration control of strain gradient nonlinear micro-cantilevers using piezoelectric actuators", *Appl. Mech. Mater.*, **789**, 976-971. <https://doi.org/10.4028/www.scientific.net/AMM.789-790.967>.
- Wang, M. and Chen, H. (2020), "Chaotic multi-swarm whale optimizer boosted support vector machine for medical diagnosis", *Appl. Soft Comput.*, **88**, 105946. <https://doi.org/10.1016/j.asoc.2019.105946>.
- Wang, M., Chen, H., Yang, B., Zhao, X., Hu, L., Cai, Z., Huang, H. and Tong, C. (2017), "Toward an optimal kernel extreme learning machine using a chaotic moth-flame optimization strategy with applications in medical diagnoses", *Neurocomputing*, **267**, 69-84. <https://doi.org/10.1016/j.neucom.2017.04.060>.
- Wang, A., Chen, H., Hao, Y. and Zhang, W. (2018), "Vibration and bending behavior of functionally graded nanocomposite doubly-curved shallow shells reinforced by graphene nanoplatelets", *Results Phys.*, **9**, 550-559. <https://doi.org/10.1016/j.rinp.2018.02.062>.
- Wu, H., Kitipornchai, S. and Yang, J. (2017), "Thermal buckling and postbuckling of functionally graded graphene nanocomposite plates", *Mater. Des.*, **132**, 430-441. <https://doi.org/10.1016/j.matdes.2017.07.025>.
- Xu, X. and Chen, H.L. (2014), "Adaptive computational chemotaxis based on field in bacterial foraging optimization", *Soft Comput.*, **18**(4), 797-807. <https://doi.org/10.1007/s00500-013-1089-4>.
- Xu, Y., Chen, H., Luo, J., Zhang, Q., Jiao, S. and Zhang, X. (2019), "Enhanced Moth-flame optimizer with mutation strategy for global optimization", *Inf. Sci.*, **492**, 181-203. <https://doi.org/10.1016/j.ins.2019.04.022>.
- Yang, J., Wu, H. and Kitipornchai, S. (2017), "Buckling and postbuckling of functionally graded multilayer graphene platelet-reinforced composite beams", *Compos. Struct.*, **161**, 111-118. <https://doi.org/10.1016/j.compstruct.2016.11.048>.
- Yas, M., Pourasghar, A., Kamarian, S. and Heshmati, M. (2013), "Three-dimensional free vibration analysis of functionally graded nanocomposite cylindrical panels reinforced by carbon nanotube", *Mater. Des.*, **49**, 583-590. <https://doi.org/10.1016/j.matdes.2013.01.001>.
- Zaoui, F.Z., Ouinas, D. and Tounsi, A. (2019), "New 2D and quasi-3D shear deformation theories for free vibration of functionally graded plates on elastic foundations", *Compos. Part B Eng.*, **159**, 231-247. <https://doi.org/10.1016/j.compositesb.2018.09.051>.
- Zarga, D., Tounsi, A., Bousahla, A.A., Bourada, F. and Mahmoud, S. (2019), "Thermomechanical bending study for functionally graded sandwich plates using a simple quasi-3D shear deformation theory", *Steel Compos. Struct., Int. J.*, **32**(3), 389-410. <https://doi.org/10.12989/scs.2019.32.3.389>.
- Zhao, X., Li, D., Yang, B., Ma, C., Zhu, Y. and Chen, H. (2014), "Feature selection based on improved ant colony optimization for online detection of foreign fiber in cotton", *Appl. Soft Comput.*, **24**, 585-596. <https://doi.org/10.1016/j.asoc.2014.07.024>.
- Zhao, X., Zhang, X., Cai, Z., Tian, X., Wang, X., Huang, Y., Chen, H. and Hu, L. (2019), "Chaos enhanced grey wolf optimization wrapped ELM for diagnosis of paraquat-poisoned patients", *Comput. Biol. Chem.*, **78**, 481-490. <https://doi.org/10.1016/j.compbiolchem.2018.11.017>

CC